Published in final edited form as:
J Am Chem Soc. 2008 August 20; 130(33): 11066–11072. doi:10.1021/ja8017303.

Role of Water in Mediating the Assembly of Alzheimer Amyloid-*β* A*β*16–22 Protofilaments

Mary Griffin Krone[†], **Lan Hua**[§], **Patricia Soto**[†], **Ruhong Zhou**[§,‖], **B. J. Berne**[§,‖], and **Joan-Emma Shea**[*,†,‡]

[†] Department of Chemistry and Biochemistry, University of California, Santa Barbara, California 93106

[§] Department of Chemistry, Columbia University, New York, New York 10027

[‖] Computational Biology Center, IBM Thomas J. Watson Research Center, 1101 Kitchawan Road, Yorktown Heights, New York 10598

[‡] Department of Physics, University of California, Santa Barbara, California 93106

Abstract

The role of water in promoting the formation of protofilaments (the basic building blocks of amyloid fibrils) is investigated using fully atomic molecular dynamics simulations. Our model protofilament consists of two parallel *β*-sheets of Alzheimer Amyloid-*β* 16–22 peptides (Ac-K^{16}-L^{17}-V^{18}-F^{19}-F^{20}-A^{21}-E^{22}-NH_2). Each sheet presents a distinct hydrophobic and hydrophilic face and together self-assemble to a stable protofilament with a core consisting of purely hydrophobic residues (L^{17},F^{19},A^{21}), with the two charged residues (K^{16}, E^{22}) pointing to the solvent. Our simulations reveal a subtle interplay between a water mediated assembly and one driven by favorable energetic interactions between specific residues forming the interior of the protofilament. A dewetting transition, in which water expulsion precedes hydrophobic collapse, is observed for some, but not all molecular dynamics trajectories. In the trajectories in which no dewetting is observed, water expulsion and hydrophobic collapse occur simultaneously, with protofilament assembly driven by direct interactions between the hydrophobic side chains of the peptides (particularly between F–F residues). For those same trajectories, a small increase in the temperature of the simulation (on the order of 20 K) or a modest reduction in the peptide–water van der Waals attraction (on the order of 10%) is sufficient to induce a dewetting transition, suggesting that the existence of a dewetting transition in simulation might be sensitive to the details of the force field parametrization.

Introduction

Proteins play a critical role in most cellular processes, from signal transduction to enzyme catalysis. Folding to the correct three-dimensional native state is crucial to their function. Under pathological conditions, proteins can misfold, typically to structures in which the hydrophobic residues, which form the hydrophobic core of the folded protein, are exposed to the solvent. These misfolded proteins can self-assemble into a variety of aggregate

[*] shea@chem.ucsb.edu .

Supporting Information Available: Two movies depicting the assembly of the peptide layers in the presence and absence of attractive solute–solvent van der Waals interactions and several figures showing the behavior of the number of interlayer waters as a function of time and interplate distance (including behavior when different parts of the force field are turned off or scaled) are provided. This material is available free of charge via the Internet at http://pubs.acs.org.

structures, including large, insoluble fibrillar entities known as amyloids. A number of diseases, including Alzheimer's disease (AD) and type II diabetes, are associated with the presence of amyloid. The proteins involved in amyloid diseases are dissimilar, in both sequence and fold, yet the end products of aggregation bear striking structural similarities including a fibrillar structure and cross-β X-ray diffraction pattern.[1-3] Because many proteins which are not associated with disease have been shown to form amyloid fibrils, it has been suggested that under certain conditions, any protein is capable of forming an amyloid.[4]

Amyloid fibrils are comprised of several protofilaments, which consist of two or more layers of β-sheets. In the specific case of the Amyloid-beta (Aβ) peptide associated with AD, both the small and large mature aggregates have shown cytotoxicity,[5] indicating the importance of studying various stages of the fibril growth process. The protofilaments grow in two manners, longitudinally, by addition of monomer proteins at their extremities,[6] and laterally, by addition of β-sheet layers.[7] This paper aims at a theoretical investigation of the role of water (the "hydrophobic effect") in mediating the lateral formation of protofilaments. Although it is well accepted that the hydrophobic effect plays a significant role in protein self-assembly in water, the precise mechanism by which it operates, as well as the exact role of water in facilitating this assembly, remains controversial. When two strongly hydrophobic surfaces, greater than 1 nm in length (such as would be the case for the extended β-sheets of a protofilament), are brought together to a critical distance, it has been suggested that a dewetting transition occurs between the two surfaces and the resulting vacuum drives the subsequent self-assembly or hydrophobic collapse. This scenario has been anticipated theoretically,[8,9] and the critical role of dewetting in the hydrophobic effect has been studied using analytical theories and simulations of simple solutes[10–21] as well as simulations of more evolved protein systems.[22,23] In general, it is nontrivial for the protein complexes to display a nanoscale dewetting transition, since it requires two or more extended hydrophobic surfaces facing each other. Therefore, it is only anticipated in the final stage of protein complex folding, once each unit has been formed and the final hydrophobic collapse is occurring.[22,23]

Alternatively, it has been suggested that the role of water in assembly would be "lubrication": in this scenario, water would not drive assembly but rather facilitate proper packing of the hydrophobic surfaces in the final stages of assembly. Such a lubrication picture has been observed in coarse-grained and fully atomistic simulations of the formation of the hydrophobic core src-SH3 protein.[24–26] To the best of our knowledge, the role of water in protofilament assembly, be it related to a dewetting transition, a lubrication effect, or other, has not yet been studied using fully atomistic simulations.

Our simulations focus on a model system consisting of the Aβ16–22 peptide (Ac-K^{16}-L^{17}-V^{18}-F^{19}-F^{20}-A^{21}-E^{22}-NH_2), the shortest fragment of the Aβ peptide capable of aggregating into fibrils. The self-assembly of the Aβ peptide is implicated in Alzheimer's disease, a debilitating neurodegenerative disease, in which atrophy of the brain leads to functional and behavioral disturbances.[27] There is increasing experimental evidence that the production and accumulation of the A β peptide is essential to the pathogenesis of AD.[28]

The Aβ16–22 peptide consists of a purely hydrophobic core (LVFFA) flanked by two oppositely charged residues (K and E). Solid state NMR experiments by Tycko and co-workers indicate that the peptides comprising the Aβ16–22 protofilament are oriented in an antiparallel manner, with interpeptide separation within a β-sheet layer of 0.47 nm and an interlayer separation between two β-sheet layers of 0.99 nm.[29] Our earlier computational work on the Aβ16–22 protofilament, using a fully atomic protein model in explicit solvent, [30] established that the most stable protofilament consists of parallel β-sheets composed of

anti parallel Aβ16–22 β-strands, such that the charged side chains (K^{16} and E^{22}) point toward the solvent, while the L^{17}, F^{19}, and A^{21} residues form the hydrophobic interior of the protofilament. In the present work, we consider a model protofilament consisting of two relatively stable, parallel, flat β-sheets, each composed of nine anti parallel A β16–22 β-strands (see Figure 1a,b). Each β-sheet is approximately 3 nm long and 2 nm wide. When separated, each sheet has one strongly hydrophobic surface and one hydrophilic surface. Because of the size of the hydrophobic surface in this system (greater than 1 nm), the clear distinction between the hydrophobic and hydrophilic surfaces of each sheet, and the strongly hydrophobic character of the interacting residues, the Aβ16–22 protofilament is an ideal biological system in which to study hydrophobic collapse; it possesses the underlying characteristics of hydrophobic plates as well as the complexities associated with proteins.

In this work we probe the possibility of a dewetting transition associated with hydrophobic collapse of two β-sheets to form the Aβ16–22 protofilament. We use a fully atomic protein representation in explicit water (see "Model and Methods" for full detail) in conjunction with both constrained and unconstrained molecular dynamics (MD). Unconstrained simulations were performed at initial intersheet separations close to or below the critical distance of dewetting at various conditions, which allow us to observe the collapse of the two sheets to form the protofilament. To investigate the possible driving forces of the observed hydrophobic collapse, we perform MD simulations to examine the contributions of the van der Waals and electrostatic components of the Hamiltonian as well as the temperature. Our results show that both the protein–water van der Waals interaction and the temperature strongly influence how water mediates the assembly of the Aβ16–22 protofilament.

Results

Hydrophobic Collapse of the Protofilament

At 300 K, "wetting" simulations (with the intersheet region initially dry) and "dewetting" simulations (with the intersheet region initially wet) were performed at various peptide β-sheet separations with the peptides positionally restrained and the water free to move about. The purpose of these simulations is to determine the dewetting critical distance, D_c. When the intersheet separation is less than D_c, water molecules will be expelled from the interior of the two positionally restrained sheets in a dewetting simulation and the interior region will remain dry in a wetting simulation. At separations greater than D_c, the interior will remain hydrated in a dewetting simulation and become hydrated in a wetting simulation.[21] At D_c, a dry interior should fluctuate between the wet and dry states with a large free energy barrier separating these states. If the barrier is sufficiently large a dry interior should remain dry and a solvated interior should remain wet during a finite time MD run. Finding an approximate value of D_c is critical for subsequent unconstrained MD simulations which should begin at an initial intersheet separation, D_0, close to or below D_c, in order to observe collapse on a relatively short time scale. For this system, D_c is found to be approximately 1.28 nm. In dewetting simulations (Figure 2a and Supporting Information), even at the shortest intersheet distances tested, the number of water molecules in the intersheet region decreases slowly with time but never approaches zero; a complete dewetting transition does not occur. This apparent lack of a dewetting transition may be due to the fact that the protein sheets are held in a fixed geometry which is slightly different from the optimal geometry observed in a long unconstrained MD simulation.[30] Trapped water could result from the improper packing of the rough surface formed by the amino acid side chains at the interior of the two protein sheets.

Next, we perform unconstrained MD simulations, in which the two sheets are initially separated by a distance, D_0, of 1.28 nm, which is close to D_c. Simulations are performed

with multiple sets of initial coordinates, each with different initial velocities. These simulations show that, after being separated, solvated in explicit water molecules, and minimized, the two sheets of the Aβ16–22 protofilament will expel all water molecules between themselves and reassociate on a time scale of ~200 ps (Figure 2b). A two-speed collapse, as observed during the assembly of two hydrophobic nanoscale oblate plates,[21] is not seen in this system. Figure 1a,b show a typical starting structure after solvation and minimization, and Figure 1c,d, after 1000 ps when most waters have been expelled (the remaining water molecules are at the edge of the protofilament). During the course of our 1000 ps MD simulations we do not observe disassembly of the protofilament and no significant distortion of the sheets is observed other than the twisting of the sheets which we observed in our earlier simulations.[30]

To investigate whether dewetting induces hydrophobic collapse, the number of waters in the intersheet region versus the intersheet distance was plotted for four representative trajectories obtained at D_c (Figure 3a-d, with additional trajectories shown in the Supporting Information). If the expulsion of water drives the collapse, we expect to see a dramatic decrease in the number of water molecules followed by a decrease in the intersheet distance. In some of the trajectories (Figure 3a,b) water expulsion does not appear to drive the collapse, and the number of intersheet water molecules decreases simultaneously with the intersheet distance. However, other trajectories (Figure 3c,d) do show a decrease in water number followed by a decrease in intersheet distance. From these plots, we can conclude that it is possible for drying to precede collapse in this system; in some instances, dewetting plays a role in protofilament self-assembly.

Decreasing the peptide–water van der Waals interactions induces a dewetting transition

It has been observed previously that the existence of a dewetting transition is sensitive to the strength of solute–solvent attractions; by turning off various components of protein–water attraction, a dewetting transition becomes more pronounced or emerges in a system which, unaltered, does not show such a transition.[21,31,32]

To determine the effect of peptide–water van der Waals interaction on the hydrophobic collapse of the β-sheets, we turned off the van der Waals attraction between water and solute. Wetting and dewetting simulations show that D_c is increased from ~1.28 nm to ~2.38 nm. Such an increase in D_c upon removing solute–solvent attractive forces has been noted previously.[32] In these simulations we observe complete dehydration of the intersheet region during the positionally restrained wetting and dewetting simulations, indicative of a dewetting transition (Supporting Information). Moreover, unconstrained MD simulations show a much faster and more dramatic collapse of the two sheets when this interaction is turned off (Supporting Information), as well as a distinct decrease in the interlayer water number followed by a decrease in the interlayer distance (Figure 3e–h, with additional trajectories shown in the Supporting Information). To determine how sensitive this strong dewetting transition is to the strength of the van der Waals attraction, we scaled the protein–water van der Waals attraction by a factor of λ^a, between 1.0 and 0.6, while keeping the protein–water van der Waals r^{-12} interaction unchanged (see Model and Methods) and using a constant value of D_0 = 1.28 nm. Figure 4a,b show that for two separate starting structures (which did not show dewetting when the full potential was used), when λ^a is decreased to approximately 90% of its original value, a dewetting transition is observed, indicating that the action of water is causing the peptide layers to come together. Scaling both the van der Waals attraction and repulsion shows a similar effect and is discussed in detail in the Supporting Information.

Turning off peptide–water electrostatic interactions does not alter the assembly mechanism

In a similar manner, the electrostatic interaction between the peptide and water was completely turned off while maintaining the van der Waals interactions on. We found D_c to be roughly 1.38 nm, slightly larger than that for the full potential. In contrast to the dramatic effect of turning off only the van der Waals attractions, turning off the protein water electrostatic interactions has a minor effect on the critical distance of the dewetting transition, consistent with the previous findings.[32] Figure 3i–l (with additional trajectories shown in the Supporting Information) show the number of waters between the peptide layers versus interlayer distance for four unconstrained MD simulations. We find almost the same dewetting behavior in the system with protein–water electrostatic interactions turned off as we do in the system with the full electrostatic interaction on; i.e., some trajectories (Figure 3i,j) show no evidence of a dewetting transition while others (Figure 3k,l) do. This is probably due to the fact that the charged amino acids (K^{16} and E^{22}) in each layer are facing away from the other layer; thus the interlayer electrostatic interaction is due primarily to the backbone atoms which are small compared to the side chain–side chain interactions (see Figure 5b).

Increasing temperature leads to a dewetting transition

Up to this point, all simulations have been performed at 300 K. It has been suggested that increasing temperature, or any other act which moves the bulk water toward liquid–gas coexistence, strengthens hydrophobic forces among large solutes19,[33] and decreases the (de)solvation free energy.[18,34] Although the temperature dependence of the dewetting-like phase behavior of single globular proteins has been studied,35 this issue has not been fully explored with respect to the hydrophobic collapse of multiple proteins or multidomain proteins. To test the effect of increased temperature on the possible dewetting of our system, we increased the temperature in 10 K increments from 300 to 370 K using the full potential with the same set of initial configurations as shown in Figure 3a,b, with D_0 = 1.28 nm. Figure 4c,d show two trajectories that did not appear to exhibit a dewetting transition at 300 K but appear to show a dewetting transition at temperatures as low as 320 K. We see that making a small increase in temperature appears to alter the mechanism for hydrophobic collapse.

What drives protofilament assembly? An Energetic Analysis

In order to probe the driving force for the interlayer association in the case of the full potential, we analyzed various components of the nonbonded contributions to the potential energy function during an unconstrained MD trajectory after the system underwent a 100 ps equilibration in which the protein is positionally restrained and water molecules are allowed to relax. A representative plot comparing various potential energy components is shown in Figure 5. First, we compared the water–water, water–peptide, and interlayer peptide–peptide components of the potential energy (Figure 5a) and conclude that there is negligible change in solvent–solvent and peptide–solvent energy brought on by the interlayer association. Conversely, the peptide–peptide potential energy from the interaction between the two peptide layers clearly decreases over the same time scale as association occurs. To further probe the source of this energetic decrease, we partition the potential energy function into terms associated with the backbone atoms (C, O, N, H), the internal-facing side chains (L^{17}, F^{19}, A^{21}), and external-facing side chains (K^{16}, V^{18}, F^{20}, E^{22}). It is clear (Figure 5b) that interactions among the internal-facing side chains of the two layers contribute most to the interlayer potential energy. Finally (Figure 5c) we plot the contributions of the specific internal-facing side chains. Clearly, the F^{19}–F^{19} and L^{17}–F^{19} interactions are the strongest and, therefore, contribute an alternative driving force to the self-assembly of the protofilament sheets. The importance of F–F interactions in protein aggregation has been

emphasized in the experimental work of Gazit and co-workers,[36] and the F–F packing in our system is shown explicitly in Figure 1d.

Discussion and Conclusion

The nature of the hydrophobic effect can differ depending on the size of the solute studied.[18,19,31,37–39] Water can accommodate small nonpolar solutes without significant disruption to its hydrogen-bond network, whereas, for large solutes (>1 nm) such as our Aβ16–22 model protofilament, persistence of such a hydrogen bond network is geometrically impossible and hence some hydrogen bonds have to be lost. In 1995 it was shown by simulation that when two strongly hydrophobic nanoscale plates are brought together to a separation sterically allowing more than one layer of water between them, the water is expelled.[10] This dewetting transition gives rise to the very strong driving force for hydrophobic collapse. These observations have been confirmed by subsequent simulations[13,15,17,21] and by theory.[9,19] A dramatic water drying transition was also observed inside the nanoscale channel formed by the melittin tetramer[23] due to the protein surface hydrophobicity and topology. Furthermore, several other proteins within the protein data bank were found to display dewetting transitions at the end stage of folding.[22] However this dewetting effect goes away when the attractive forces between solute and water are made sufficiently strong.[31,32,40–42]

In this paper, we investigate the role of a drying or dewetting transition in the formation of a protofilament from aggregating Alzheimer Aβ16–22 peptides. Our protofilament consists of two antiparallel β-sheets, each with one highly hydrophobic side (the “interior side” composed of the L^{17}, F^{19}, and A^{21} residues). Because of their high stability and strongly hydrophobic character, the β-sheets resemble two hydrophobic plates. However, in contrast to the idealized hydrophobic species studied previously, the peptide backbone causes this system to stray from being fully hydrophobic; even the most hydrophobic regions in proteins have weak polarity and significant dispersion interactions.

The bilayer protofilaments formed by the Aβ16–22 peptide have dry interfaces once assembled. This is a result of both the close packing of the interior side chains and the fact that these side chains (L^{17}, F^{19}, A^{21}) are neutral, hydrophobic molecules. In the case of longer fragments of the Aβ peptide, such as the Aβ9–40[43] and Aβ17–42[44] fragments, hydrated hydrophobic cavities have been reported in molecular dynamics simulations.[43,44] These peptides adopt a β-strand-loop-β-strand U-shape in the fibril (in contrast to the simple β-strand arrangement seen here). In both Aβ9–40 and Aβ17–42 protofilaments, water is observed in the mostly hydrophobic cavity formed by the loop region. The water filling these cavities may play a role in enhancing fibril stability, by neutralizing the charges inside the core of the fibril (in the case of the Aβ9–40 peptide, the D^{23} and K^{28} charges). Interestingly, short aggregating peptides that are rich in polar residues, such as the GNNQQNY fragment of the yeast protein Sup35, can form both dry and wet interfaces.[45] The dry interface results in this case primarily from the unique shape complementary of the polar side chains.

Our results show that after being separated by a distance equal to approximately the dewetting critical distance, D_c, the two sheets of the Aβ16–22 protofilament will self-assemble on a time scale of ~200 ps (Figure 2b). The time scale for this hydrophobic collapse is long compared to the ideally hydrophobic oblate plates which fully associate in approximately 30 ps;[21] however it is approximately equal to the time scale of hydrophobic collapse for the melittin protein tetramer[23] and faster than the BphC enzyme[32] which associates in ~1000 ps. This result implies the time scale of dewetting events for complex,

evolved systems such as proteins which include solute–solvent attraction is much shorter and less dramatic than that of simple hydrophobic plates.

We observe a dewetting or drying transition preceding, and in effect prompting, a hydrophobic collapse in some but not all of our simulations. Turning off the protein–water electrostatic interaction does not significantly affect this result since the intersheet surfaces consist of mostly hydrophobic residues; however a slight decrease in the assembly time (by a factor of ~2, from about 200 to 100 ps) is observed. Conversely, if we turn off the protein–water van der Waals attraction, we see a dewetting transition in every simulation. This observation is consistent with new results based on simulations of planar nanoscale hydrophobic plates composed of hexagonally packed carbon atoms.31 These simulations show that when attractive van der Waals forces exist between the solute and solvent, these forces, though individually small, can be enough to compensate for the loss of hydrogen bonds due to confinement of water between the two plates and thus prevent a dewetting transition from occurring. By varying the strength of the protein–water van der Waals attraction, we determine that decreasing these forces to approximately 90% of their original strength is significant enough to allow dewetting to occur. In a similar vein, it has been implied that increasing temperature, or any other act which moves the bulk water toward liquid–gas coexistence, strengthens hydrophobic forces among large solutes19 and decreases the (de)solvation free energy.18,34 Indeed, upon increasing the temperature of our simulations even by just 20 K, we do observe a dewetting transition. These results show how small parameter changes can lead to the emergence of a dewetting transition.

As mentioned, a dewetting transition is observed only in some of the trajectories (based on the original potential energy function), yet the peptide layers always self-assemble; thus, dewetting induced collapse is not the only force in protofilament association, at least for this potential. In the trajectories that do not display a dewetting transition, water appears to play a “lubricating” role rather than serve as a driving force for collapse. The imperfect packing of the protofilament core leads to trapped water molecules that are expelled from the wet core along with the collapse of the protofibril. An analysis of the contributions of various components to the potential energy between the peptide layers (Figure 5) indicates that the interactions between the hydrophobic side chains of the two layers (L^{17}, F^{19}, A^{21}), specifically the F–F and F–L interactions, contribute most to the decrease in potential energy which is observed over the same time frame as the association. Hence direct favorable energetic interactions between hydrophobic side chains are in some instances sufficient to drive protofilament assembly and lead to the expulsion of the water molecules.

The simulations presented in this paper highlight the subtle interplay between water mediated collapse of the protofilament and collapse driven by specific side chain interactions. It is noteworthy that very minor changes in the simulation temperature (by only 20 K) and the force field parameters (reducing the van der Waals solvent–solute attraction by only 10%) are sufficient to induce a dewetting transition in trajectories in which assembly appeared to be driven primarily by direct protein–protein interactions. The implication of this finding is that the presence or absence of a dewetting transition in simulation is extremely sensitive to the precise details of force fields, highlighting the critical role of the parametrization of protein–solvent interactions in modern force fields.

Model and Methods

Our previous studies of Aβ16–22 protofilaments[30] reveal that the peptides adopt a primarily antiparallel arrangement, consistent with other experimental[29] and theoretical[46–49] investigations. Our model protofilament consists of two parallel β-sheets, each composed of nine antiparallel Aβ16–22 β-strands, as shown in Figure 1a,b. After running two different

100 ns long simulations, we did not observe a significant number of water molecules at the interior of the protofilament.[30] The initial center of mass separation (calculated over backbone atoms) between the two β-sheets was 0.78 nm and ranged from 0.89 to 0.95 nm during the course of our two 100 ns simulations. The initial separation between individual peptide chains in a sheet was 0.44 nm and had an average value of 0.47 nm. Both sheet and strand separation distances are consistent with values reported from solid state NMR data (0.99 and 0.47 nm, respectively).

Here, we use the same initial structure that we used for our 100 ns simulations. The peptides are solvated in a periodic cubic box of simple point charge (spc)50 water molecules with a minimum distance between the peptide and the edge of the box of at least 0.8 nm; the structure does not interact with its periodic image. All water molecules that overlapped with the peptide were deleted, and a steepest descent energy minimization was performed for 500 steps. The GROMOS96 force field51 was used to describe the solute. The temperature was maintained close to 300 K (unless otherwise stated) by weak coupling to an external temperature bath52 with a coupling constant of 0.1 ps. The LINCS algorithm53 was used to constrain bond lengths within the solute, while the SETTLE algorithm54 was used to constrain the bond lengths and angle in water. The integration time step was 2 fs, and snapshots were saved every picosecond. A cutoff of 0.9 nm was used to evaluate the nonbonded interactions. Fast Particle-Mesh Ewald (PME)55 electrostatics were used with calculations in direct space similar to the Classical Ewald sum electrostatic, while the reciprocal part was performed with FFTs with a maximum grid spacing of 0.12 nm and a cubic interpolation. The relative strength of the Ewald shifted direct potential at the cutoff is 10^{-5}. All simulations were performed using the GRO-MACS3.2 software package.[56,57]

Following solvation and minimization, “wetting” and “dewetting” simulations were performed for 1 ns each at five peptide β-sheet separation distances with the peptide positionally restrained and the waters free to move about. The intersheet distance is the distance between the center of mass (calculate over backbone atoms) of the two sheets. The purpose of these simulations is to find the dewetting critical distance, D_c.[21] For the wetting simulations, all water molecules were removed from the intersheet region following equilibration. Water molecules were counted as being between the sheets if the combined distance between the water (oxygen atom) and the closest α-carbon in each of the two β-sheets ($C\alpha_1$ and $C\alpha_2$) is less than the distance between the two sheets (as determined by the distance between $C\alpha_1$ and $C\alpha_2$) to within a tolerance of 0.2 nm. The number of intersheet water molecules is calculated using the same criteria.

After determining D_c from the wetting and dewetting simulations, a single initial intersheet separation, D_0, was used for unconstrained MD simulations. Independent simulations (12) were performed with different initial coordinates and/or velocities at 300 K. For eight of these starting points, additional simulations were performed at temperatures in 10 K intervals between 300 and 370 K for a total of 56 additional simulations. We did not observe a change in D_c for these high temperature simulations.

We turned off the van der Waals protein–water attraction by setting the C_6 coefficient ($V_{vdw} = C_{12}(1/r)^{12} - C_6(1/r)^6$ where $C_{12} = 4\epsilon\sigma^{12}$ and $C_6 = 4\epsilon\sigma^6$) to zero for all interactions between the water and protein. Again, 5 wetting and dewetting simulations were performed at various intersheet separations, and 12 unconstrained MD simulations were performed at the chosen value of D_0. For eight of these starting points, the C_6 coefficient was scaled by a factor of λ^a ($V_{vdw} = \lambda^r C_{12}(1/r)^{12} - \lambda^a C_6(1/r)^6$) equal to 0.05, 0.6, 0.7, 0.8, and 0.9 for an additional 40 simulations. This procedure was repeated scaling both the C_6 and C_{12} coefficients corresponding to protein–water van der Waals attraction and repulsion, by λ^a and λ^r, respectively.

Finally, we turned off the protein–water electrostatic interaction. This was done using a simpler procedure than the PME method; the direct protein–water electrostatic interaction was turned off, and the remaining electrostatic interaction was treated using a spherical cutoff of 1.3 nm. The use of a spherical cutoff of 13 Å instead of PME was tested on the full interaction potential, and it was found that both the PME and spherical cutoff approximation predicted the same critical distance for dewetting.

Supplementary Material

Refer to Web version on PubMed Central for supplementary material.

Acknowledgments

This work was supported in part by an NIH grant (GM43340) to B.J.B. Support from the NSF (No. MCB 0642086 to J.E.S.) and the David and Lucile Packard Foundation (to J.E.S.) are gratefully acknowledged. Simulations were performed using the TACC Lonestar Cluster (NSF Teragrid MCA05S027). R.Z. would like to thank the IBM BlueGene science program for support.

References

(1). Teplow DB. Amyloid. 1998; 5:121–142. [PubMed: 9686307]
(2). Sunde M, Blake C. AdV. Protein Chem. 1997; 50:123–159. [PubMed: 9338080]
(3). Eanes ED, Glenner GG. J. Histochem. Cytochem. 1968; 16:673–677. [PubMed: 5723775]
(4). Dobson CM. Trends Biochem. Sci. 1999; 24:329–332. [PubMed: 10470028]
(5). Caughey B, Lansbury PT. Annu. ReV. Neurosci. 2003; 26:267–298. [PubMed: 12704221]
(6). Tseng BP, Esler WP, Clish CB, Stimson ER, Ghilardi JR, Vinters HV, Mantyh PW, Lee JP, Maggio JE. Biochemistry. 1999; 38:10424–10431. [PubMed: 10441137]
(7). Nichols MR, Moss MA, Reed DK, Lin W-L, Mukhopadhyay R, Hoh JH, Rosenberry TL. Biochemistry. 2002; 41:6115–6127. [PubMed: 11994007]
(8). Berard DR, Attard P, Patey GN. J. Chem. Phys. 1993; 98:7236–7244.
(9). Patey GN. Ber. Bunsen-Ges. Phys. Chem. 1996; 100:885–888.
(10). Wallqvist A, Berne BJ. J. Phys. Chem. 1995; 99:2893–2899.
(11). Li X, Li J, Eleftheriou M, Zhou R. J. Am. Chem. Soc. 2006; 128:12439–47. [PubMed: 16984193]
(12). Zangi R, Hagen M, Berne BJ. J. Am. Chem. Soc. 2007; 129:4678–86. [PubMed: 17378564]
(13). Lum K, Luzar A. Phys. ReV.E. 1997; 56:R6283–R6286.
(14). Hummer G, Garde S. Phys. ReV. Lett. 1998; 80:4193–4196.
(15). Luzar A, Leung K. J. Chem. Phys. 2000; 113:5836–5844.
(16). Ashbaugh HS, Paulaitis ME. J. Am. Chem. Soc. 2001; 123:10721–10728. [PubMed: 11674005]
(17). Bratko D, Curtis RA, Blanch HW, Prausnitz JM. J. Chem. Phys. 2001; 115:3873–3877.
(18). Huang DM, Chandler D. J. Phys. Chem. B. 2002; 106:2047–2053.
(19). Lum K, Chandler D, Weeks JD. J. Phys. Chem. B. 1999; 103:4570–4577.
(20). Wallqvist A, Gallicchio E, Levy RM. J. Phys. Chem. B. 2001; 105:6745–6753.
(21). Huang X, Margulis CJ, Berne BJ. Proc. Natl. Acad. Sci. U.S.A. 2003; 100:11953–11958. [PubMed: 14507993]
(22). Hua L, Huang X, Liu P, Zhou R, Berne BJ. J. Phys. Chem. B. 2007; 111:9069–9077. [PubMed: 17608515]
(23). Liu P, Huang XH, Zhou RH, Berne BJ. Nature. 2005; 437:159–162. [PubMed: 16136146]
(24). Cheung MS, Garcia AE, Onuchic JN. Proc. Natl. Acad. Sci. U.S.A. 2002; 99:685–690. [PubMed: 11805324]
(25). Guo W, Lampoudi S, Shea J-E. Biophys. J. 2003; 85:61–69. [PubMed: 12829464]
(26). Shea J-E III. Proc. Natl. Acad. Sci. U.S.A. 2002; 99:16064–16068. [PubMed: 12446834]

(27). Cummings JL. N. Engl. J. Med. 2004; 351:56–67. [PubMed: 15229308]
(28). Hardy J, Selkoe DJ. Science. 2002; 297:353–356. [PubMed: 12130773]
(29). Balbach JJ, Ishii Y, Antzutkin ON, Leapman RD, Rizzo NW, Dyda F, Reed J, Tycko R. Biochemistry. 2000; 39:13748–13759. [PubMed: 11076514]
(30). Soto P, Griffin MA, Shea J-E. Biophys. J. 2007; 93:3015–3025. [PubMed: 17631541]
(31). Choudhury N, Pettit BM. J. Am. Chem. Soc. 2005; 127:3556–3567. [PubMed: 15755177]
(32). Zhou RH, Huang XH, Margulis CJ, Berne BJ. Science. 2004; 305:1605–1609. [PubMed: 15361621]
(33). Wolde, P. R. t.; Chandler, D. Proc. Natl. Acad. Sci. U.S.A. 2002; 99:6539–6543. [PubMed: 11983853]
(34). Huang DM, Chandler D. Proc. Natl. Acad. Sci. U.S.A. 2000; 97:8324–8327. [PubMed: 10890881]
(35). Finkelstein EV, Shaknovich EI. Biopolymers. 1989; 28:1681–1694. [PubMed: 2597724]
(36). Azriel R, Gazit E. J. Biol. Chem. 2001; 276:34156–34161. [PubMed: 11445568]
(37). Cheng YK, Rossky PJ. Nature. 1998; 392:696–699. [PubMed: 9565030]
(38). Lee CY, McCammon JA, Rossky PJ. J. Chem. Phys. 1984; 80:4448–4454.
(39). Southall NT, Dill KA. J. Phys. Chem. B. 2000; 104:1326–1331.
(40). Choudhury N, Pettit BM. J. Am. Chem. Soc. 2007; 129:4847–4852. [PubMed: 17385863]
(41). MacCallum JL, Moghaddam MS, Chan HS, Tieleman DP. Proc. Natl. Acad. Sci. U.S.A. 2007; 104:6206–6219. [PubMed: 17404236]
(42). Ma B, Nussinov R. Proc. Natl. Acad. Sci. U.S.A. 2002; 99:14126–31. [PubMed: 12391326]
(43). Buchete NV, Tycko R, Hummer G. J. Mol. Biol. 2005; 353:804–21. [PubMed: 16213524]
(44). Zheng J, Jang H, Ma B, Tsai CJ, Nussinov R. Biophys. J. 2007; 93:3046–57. [PubMed: 17675353]
(45). Nelson R, Sawaya MR, Balbirnie M, Madsen AO, Riekel C, Grothe R, Eisenberg D. Nature. 2005; 435:773–8. [PubMed: 15944695]
(46). Favrin G, Irback A, Mohanty S. Biophys. J. 2004; 87:3657–3664. [PubMed: 15377534]
(47). Gnanakaran S, Nussinov R, Garcia AE. J. Am. Chem. Soc. 2006; 128:2158–2159. [PubMed: 16478138]
(48). Klimov DK, Thirumalai D. Structure. 2003; 11:295–307. [PubMed: 12623017]
(49). Santini S, Wei GH, Mousseau N, Derreumaux P. Structure. 2004; 12:1245–1255. [PubMed: 15242601]
(50). Berendsen, HJC.; Postma, JPM.; van Gunsteren, WF.; Hermans, J. Intermolecular Forces. Reidel; Dordrech: 1981.
(51). Scott WRP, Hunenberger PH, Tironi IG, Mark AE, Billeter SR, Fennen J, Torda AE, Huber T, Kruger P, van Gunsteren WF. J. Phys. Chem. A. 1999; 103:3596–3607.
(52). Berendsen HJC, Postma JPM, Vangunsteren WF, Dinola A, Haak JR. J. Chem. Phys. 1984; 81:3684–3690.
(53). Hess B, Bekker H, Berendsen HJC, Fraaije JGEM. J. Comput. Chem. 1997; 18:1463–1472.
(54). Miyamoto S, Kollman PA. J. Comput. Chem. 1992; 13:952–962.
(55). Essmann U, Perera L, Berkowitz ML, Darden T, Lee H, Pedersen LG. J. Chem. Phys. 1995; 103:8577–8593.
(56). Berendsen HJC, van der Spoel D, van Drunen R. Comput. Phys. Commun. 1995; 91:43–56.
(57). Lindahl E, Hess B, van der Spoel D. J. Mol. Model. 2001; 7:306–317.

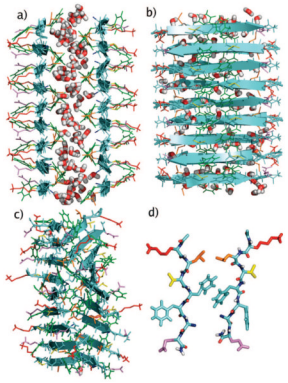

Figure 1.

Aβ16–22 model protofilament. (a and b) The initial structure used to start the MD trajectory seen in Figure 2b-i, with D_0 of 1.28 nm. Front (a) and side (b) views are shown. Side chains are colored as follows: K = red, L = orange, V = yellow, F = green, A = blue, and E = violet. For clarity, only water molecules in the interpeptide region have been shown. (c) The same structure after 1000 ps of unconstrained MD simulation at 300 K, started from the structure shown in (a and b). (d) A single Aβ16–22 peptide pair, one from each layer, is isolated from the protofilament shown in (c).

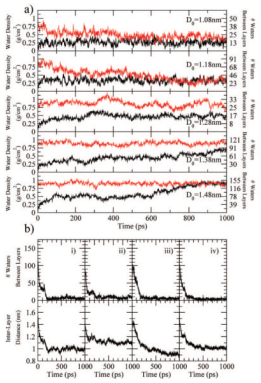

Figure 2.

Trajectory data using the full potential energy function. (a) Plots of the number density of water between the two nine-stranded peptide sheets as a function of time for wetting (black) and dewetting (red) simulations at 300 K. From these plots, D_c is determined to be ~1.28 nm. (b, Top) Plots of the number of water molecules between the two peptide sheets as a function of time for unconstrained MD simulations. Each plot shows a different trajectory with D_0 = 1.28 nm. (b, Bottom) Plots of the distance between the two peptide sheets as a function of time for nonconstrained MD simulations. Each simulation corresponds to the same trajectory as the plot above it.

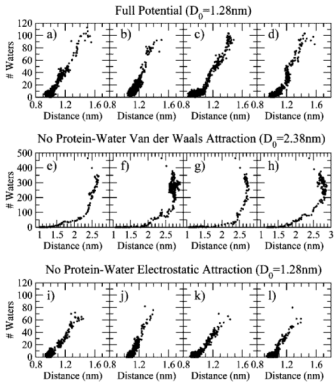

Figure 3.

Number of interpeptide water molecules versus interpeptide distance. (a–d) Plots for each of the four trajectories at 300 K shown in Figure 2b (i–iv, respectively), where D_0 = 1.28 nm. Trajectories a and b do not appear to show a dewetting transition, while trajectories c and d do. (e–h) The peptide–water van der Waals interaction is turned off, and D_0 = 2.38 nm. (i–l) The peptide–water electrostatic interaction is turned off, and D_0 = 1.28 nm.

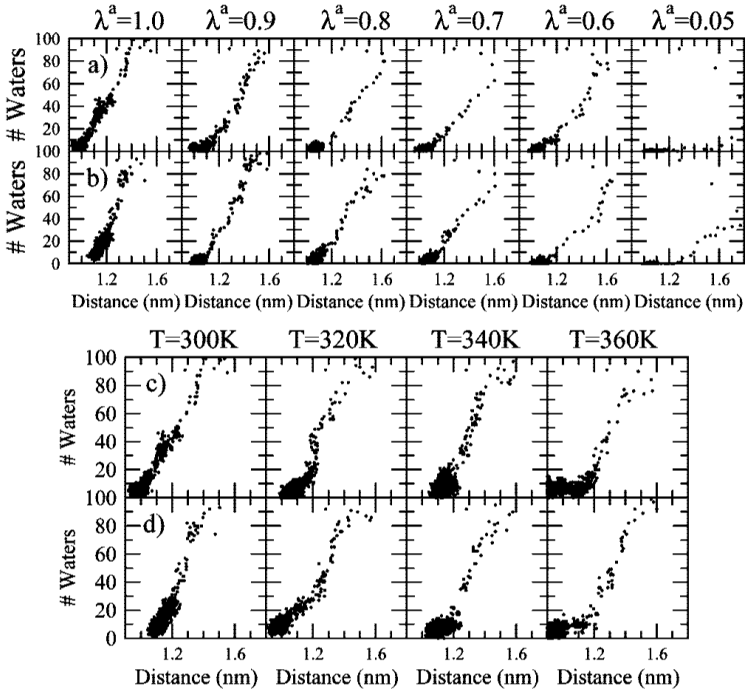

Figure 4.

Number of interpeptide water molecules is plotted against the interpeptide distance for the two trajectories in which a drying transition was not observed using the original potential function. In each simulation the initial conditions are the same as those in Figure 3a and b, D_0 is 1.28 nm, and the temperature is 300 K. (a and b) The van der Waals attraction between the peptide and water has been scaled by a factor of λ^a (such that $\lambda^a = 1$ is the full potential used in Figure 3a,b). In each case the repulsive term of the van der Waals interaction is unchanged. (c and d) Each simulation is performed at a different temperature.

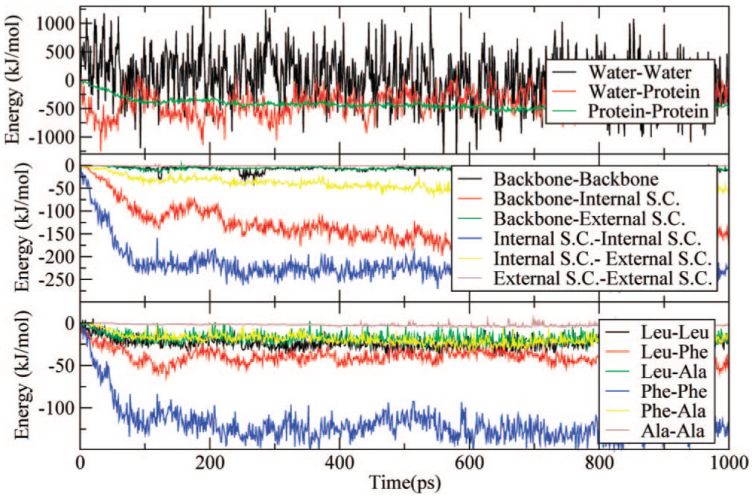

Figure 5.

A representative plot of energy versus time for an unconstrained MD trajectory at 300 K after an equilibration period of 100 ps. (a) The water–water, water–peptide, and interlayer peptide–peptide nonbonded components of the potential energy are compared. (b) The potential energy components associated with backbone atoms (C, O, N, H), the internal-facing side chains (L^{17}, F^{19}, A^{21}), and external-facing side chains (K^{16}, V^{18}, F^{20}, E^{22}) are compared. (c) The contributions of interactions among the specific internal-facing side chains are compared.